

Thi X. T. Sayle¹, Francesco Caddeo¹, Xueqiang Zhang², Tamilselvan Sakthivel³, Soumen Das³, Sudipta Seal^{3,4}, Sylwia Ptasinska⁵ and Dean C. Sayle^{1,*}

¹School of Physical Sciences, University of Kent, Canterbury, CT2 7NZ, UK

*d.c.sayle@kent.ac.uk

²Radiation Laboratory and Department of Chemistry and Biochemistry, University of Notre Dame, Notre Dame, IN 46556, USA

³Advanced Materials Processing and Analysis Center (AMPAC), NanoScience Technology Center (NSTC), Materials Science Engineering (MSE), University of Central Florida, 4000, Central Florida Boulevard, Orlando, FL 32816, USA

⁴College of Medicine, University of Central Florida, 6850 Lake Nona Blvd, Orlando, FL 32827

⁵Radiation Laboratory and Department of Physics, University of Notre Dame, Notre Dame, IN 46556, USA

ABSTRACT

Structure-activity mapping is central to the exploitation and optimisation of nanomaterial catalysts in a variety of technologically important heterogeneous reactions, such as automotive catalysis and water gas shift reactions. Here, we present a catalytic activity map for nanoceria, calculated as a function of shape, size, architecture and defect content, using atom-level models.

The activity map reveals that as oxygen is gradually depleted from the nanoceria catalyst, so it becomes energetically more difficult to extract further oxygen. We propose that the oxygen storage capacity (OSC) of ceria corresponds to the level of oxygen depletion where it becomes thermodynamically prohibitive to extract further oxygen from the material (positive free energy). Moreover, because the reaction enthalpy contributes to the free energy, we predict that the OSC is influenced by the particular reaction being performed. Specifically, the more negative the reaction enthalpy, the higher the potential OSC (notwithstanding entropic contributions).

The decrease in catalytic activity during an oxidation reaction - emanating from the increase in energy required to extract oxygen - suggests that there exists a 'window of catalytic operation', where the activity of the catalyst can be controlled by operating at different points within this window. We show experimentally, how the activity can be modified by engineering the oxygen vacancy concentration and hence the oxygen content of the catalyst to facility tunable activity.

In addition to the defect content, we find that size (particle diameter, mesoporous wall thickness) and nanostructuring (particle, cube, mesoporous architecture, morphology and surfaces exposed) are key drivers of catalytic activity.

To generate the atom-level models of ceria nanostructures, we use non-equilibrium Molecular Dynamics to simulate the self-assembly of mesoporous ceria from amorphous nano-building blocks, followed by a (simulated) crystallisation step; the latter evolves the crystal structure and microstructural features such as grain-boundaries and dislocations. Our simulated crystallisations emanate wholly from a multitude of 'random' atom collisions, which result in the spontaneous evolution of a crystalline seed that nucleates crystallisation of the whole system. The atomistic models generated by 'simulating synthesis' are shown to be in quantitative structural agreement with experiment.

INTRODUCTION

When CO is oxidised to CO₂, oxygen is extracted from the surface of the ceria catalyst.¹ Intuitively, the less energy required to extract the oxygen, the more active the catalyst towards oxidation. Indeed, oxygen vacancy formation energies have been shown to be a ‘simple yet powerful activity predictor for catalytic reactions on ceria’.² However, as oxygen is gradually extracted from the catalyst, does it become energetically more difficult to extract further oxygen? Here, we use MD simulation to calculate the change in activity of nanoceria as its oxygen content is gradually depleted or, conversely, replenished.

Sayle et al. and Conesa calculated that it is easier to extract oxygen from {310}, {110} and dipolar {100} ceria surfaces compared to {111} surfaces.^{3,4} However, these surfaces are also thermodynamically less stable than CeO₂{111}. This leaves a conundrum – how does one fabricate more active surfaces if the less active (111) surface is more stable and therefore preferentially exposed? Nanostructuring has been shown to facilitate the exposure of active ceria surfaces compared to the parent bulk material; typically, ceria nanoparticles comprise a high proportion of {100} and {110} surfaces relative to {111} surfaces.^{5,6,7,8,9} Moreover, by changing the synthetic protocol, ceria nanocubes, with six {100} surfaces, can be fabricated;^{10,11,12} such ceria nanocubes have been shown to display exemplary activity.¹³

Previously we showed, using atomistic simulation, that the energy required to extract oxygen from ceria nanoparticles is lower compared to the parent bulk material.¹⁴ This was attributed to a higher concentration of {100} and {110} surfaces relative to CeO₂{111}, compared to the parent bulk material. Calculating vacancy formation energies is computationally expensive; typically, a 10 nm ceria particle comprises about 10,000 oxygen ions. Conversely, the Madelung energy has been shown to be a good gauge of oxygen vacancy formation energy, yet requires 7 orders of magnitude less cpu.¹⁵ This enables activity ‘fingerprints’ to be calculated, fig 1, which provide a visual representation of the activity of particular facets.^{15, 16} Such activity ‘fingerprints’ reveal how the surfaces exposed, nanoarchitecture (size, shape, curvature, morphology), microstructure (dislocations and grain-boundaries) and strain influence the chemical activity. The study predicted that ceria catalysts, with low-coordinated surface oxygen, are more active towards oxidation (of, for example, CO to CO₂). In particular, the energy required to extract oxygen from a nanoparticle of ceria was calculated to be: +623 kJmol⁻¹ (bulk ceria), +453 kJmol⁻¹ (plateau {111}), +195 kJmol⁻¹ (plateau {100}), +166 kJmol⁻¹ (step on {111}) and +51 kJmol⁻¹ (apical {100}).

Tensile strain was also predicted to reduce the energy required to extract surface oxygen. However, these calculations only considered extracting oxygen from the fully oxidised (CeO_{2-x} ; $x=0$) material. Conversely, the real nanomaterial is likely to be partially reduced^{17,18} and will become further oxygen deficient as the oxidation proceeds. Indeed, Lawrence and co-workers showed that the catalytic activity of ceria can be engineered via the creation of oxygen vacancies.¹⁹

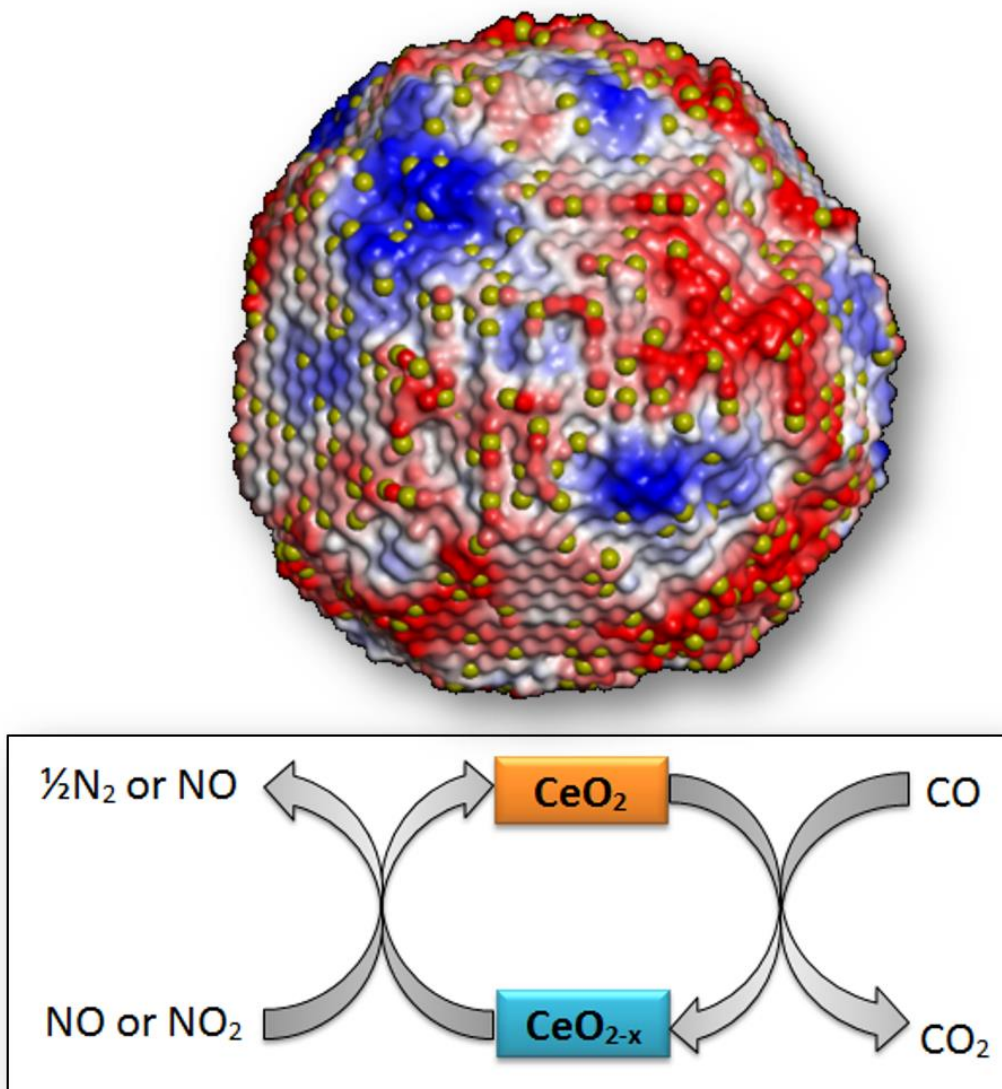


Figure 1 Schematic, illustrating the oxidation of CO to CO_2 (CeO_2 reduces to CeO_{2-x}) and reduction of NO_2 to NO (CeO_{2-x} oxidises to CeO_2). The top image shows a model ceria nanoparticle coloured according to how (energetically) facile it is to extract surface oxygen (red–white–blue: easy to difficult to extract). The yellow dots indicate the positions of Ce^{3+} ions.

The Catalytic Cycle

As ceria provides oxygen for oxidation reactions (such as: $\text{CO} + \frac{1}{2}\text{O}_2 \rightarrow \text{CO}_2$), the oxygen content of the ceria will gradually become depleted. It is therefore important to determine the activity of the ceria nanomaterial as oxygen is consumed. Specifically, does the ceria catalyst retain its activity towards oxidation as the ceria is gradually reduced? Similarly, if ceria is to act catalytically, the oxygen depleted must be replenished. This can be achieved via a reduction reaction (such as: $\text{NO}_2 - \frac{1}{2}\text{O}_2 \rightarrow \text{NO}$). It is therefore important to calculate the activity of the nanomaterial as oxygen is replenished. Specifically, does the ceria retain its activity towards reduction as the ceria is oxidised? An automotive catalytic cycle is shown in fig 1, to illustrate the two competing reactions.²⁰

Synergy of oxidative/reductive catalysis

If it is 'easy' (low oxygen vacancy formation energy) to extract an oxygen ion from a particular active surface for oxidation, then the energy associated with replacing the oxygen during reduction, will be equal in magnitude, but opposite in sign, to the vacancy formation energy. In this situation, the more active surfaces for reduction would, presumably, be those surfaces with high vacancy formation energies, such as $\text{CeO}_2\{111\}$. In particular, more energy would be released, when the vacancy was filled. Indeed, Namai and co-workers reported that oxygen vacancies, on a slightly reduced $\text{CeO}_2(111)$ surface, were healed by exposure to NO_2 .²¹ Similarly, a recent study by Vile and co-workers showed that 'whereas the (100) surface, predominantly exposed in nanocubes, is optimal for CO oxidation, the (111) surface, prevalent in conventional polyhedral CeO_2 particles, dominates in C_2H_2 hydrogenation'.²² An analogous observation was made by Roy and co-workers, who explored the photocatalytic properties of TiO_2 . In particular, a focus for nanomaterial design for photocatalysis is to increase the surface area of high-energy TiO_2 surfaces, such as {001} and {100}, to improve catalytic activity. Conversely, Roy and co-workers found that the synergistic presence of both the high-energy {001}-oxidative and low-energy {101}-reductive facets, in an optimum ratio, is necessary to reduce the charge recombination and thereby enhance photocatalytic activity of TiO_2 nanocrystals.²³

Here, we calculate the energy required to extract oxygen from nanoceria, to determine the activity of nanoceria catalysts, as the oxygen comprising the catalyst is consumed and replenished during oxidative/reductive catalytic cycles. We explore the (synergistic) influence of different facets, nanostructuring (nanoparticle, nanocube, mesoporous), microstructure (dislocations, grain-boundaries) and size (nanoparticle diameter, mesoporous wall thickness).

In the second part of the study, we engineer the defect chemistry of nanoceria by exposing the material to either oxidising or reducing conditions in a reaction chamber. In particular, we determine experimentally whether the activity predictions can be exploited to optimising the activity of the real nanomaterial.

METHODS

The Born model of the ionic solid was used to describe the nanoceria in which the component Ce and O ions interact via short-range parameterised interactions coupled with long-range Coulombic interactions. The potential parameters were taken from ref. [3] using a rigid ion model. All the MD simulations were performed using the DL_POLY code.²⁴

Generating Atomistic Models

The activity of nanoceria is governed by its hierarchical structural complexity, including the polymorphic *crystal structure*, *microstructure* (dislocations, grain-boundaries) and *nanoarchitecture* (network and connectivity of pores; morphology and surfaces exposed). Such structural complexity traverses length and timescales far greater than can currently be accommodated using electronic structure methods. Accordingly, we extend atomistic modelling to the mesoscale to generate models that capture the hierarchical structural complexity.

Atomistic models are normally generated using experimental data including atom positions derived from X-ray Diffraction (XRD) or High Resolution Transmission Electron Microscopy (HRTEM) or from chemical intuition and symmetry operators. However, such classical approaches become intractably difficult when one considers that the unit cells of nanomaterials comprise tens of thousands of atoms. Moreover, complex microstructures and nanoarchitectures, which have a profound influence on the chemical properties, are difficult to capture within an atomistic model.

Hierarchical structural complexity of the real material emanates from the synthetic protocol used in its fabrication and therefore to generate realistic models, in that they accurately reflect the real material, we ‘simulate synthesis’. In particular, we simulate the self-assembly of mesoporous ceria from nano building blocks, followed by a (simulated) crystallisation step, which evolves the crystal structure and microstructural features. In particular, during experimental synthesis, mesoporous CeO₂ emanates from an amorphous pre-cursor, which undergoes crystallisation into the mesoporous nanoform.²⁵ We simulate

directly this process: we start with amorphous precursors and allow the system to crystallise under non-equilibrium MD simulation. Analogous to experiment, we control only the temperature of the system. At a particular instant in time, under MD simulation, the combination of ‘random’ atom collisions spontaneously result in the evolution of a crystalline seed. This seed then nucleates crystallisation to facilitate the crystal structure (fluorite), the microstructure (dislocations and grain-boundaries) and nanoarchitecture (network of interconnecting pores, curved (internal) surface morphologies) in accord with experiment.²⁶ We argue that because our procedure of ‘simulating synthesis’ generates models with three levels of hierarchical structural complexity (crystal structure-microstructure-nanoarchitecture) in accord with experiment, starting from an amorphous starting point by just controlling the simulation temperature, our methodological approach is valid. Figure 2 shows graphically the basic strategy used to generate the atomistic models of mesoporous ceria. Full details, describing the generation of the atomistic models, are presented in supporting information. We now report on the structure of the atomistic models emanating from simulating synthesis.

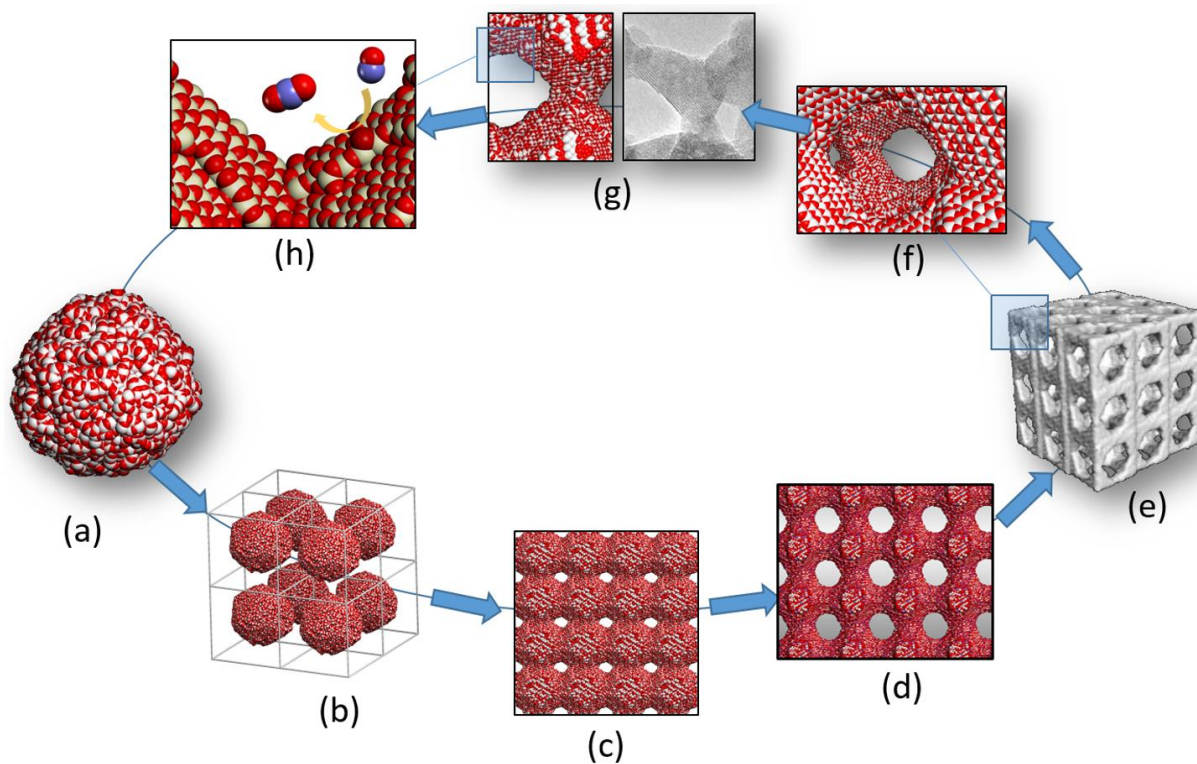


Figure 2 Strategy used to generate atom-level models of mesoporous ceria. (a) amorphous CeO_2 nanobuilding block. (b) building blocks introduced into simulation cell. (c) 'self-assembly' of nanobuilding blocks into mesoporous architecture. (d) crystallisation of system (evolution of fluorite crystal structure, grain-boundaries and dislocations). (e) Three-dimensional Connolly surface of atom positions in (d). (f) view showing the pore structure. (g) structural accord with experiment (HRTEM). (h) Oxidation of CO to CO_2 using oxygen from ceria catalyst. The images all reflect simulated atom positions; none are schematic.

Ceria Nanoparticles Analysis of the nanoparticles, using graphical techniques, reveal polyhedral morphologies with $\{111\}$ surfaces truncated by $\{100\}$, fig 3, in accord with experiment, fig S1.^{27,28} The 3.5 and 6nm particles crystallised into single crystals, while the 8 and 9nm particles comprise mis-oriented grains, separated by grain-boundaries and triple-junctions, fig S2. The structure of the ceria nanocube is presented in fig S3 and shows that the structure of the surfaces, including surface faceting, is in quantitative accord with experiment, fig S3(j-m).

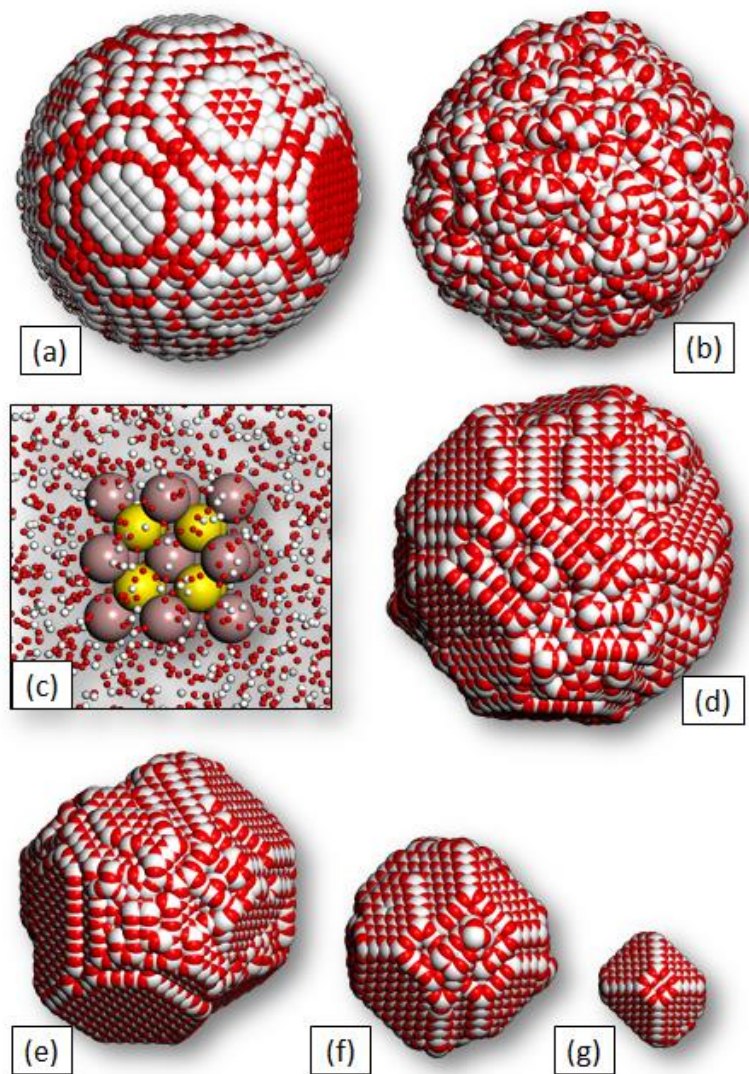


Figure 3 Atomistic models of polyhedral ceria nanoparticles. (a) Sphere cleaved from parent bulk material, (b) structure of the molten nanoparticle, (c) structure of the crystalline seed at the centre of the nanoparticle, (d) final, low-temperature structure of the crystalline nanoparticle, (d), (e), (f) and (g) are drawn to scale and represent the final structures of the 9, 8, 6 and 3.5 nm nanoparticles respectively. Cerium is coloured white and oxygen is red.

Mesoporous Ceria The structure of mesoporous ceria (model) is shown in fig 4; additional structural models are given in supporting information, figs S4-S6. Analysis of the models reveal that the pores expose predominantly $\{111\}$ surfaces with smaller domains of $\{110\}$ and $\{100\}$ in accord with experiment.²⁶ The mesoporous ceria models, with simple cubic pore structures, are in close accord with experiment: fig 4(c,d) and fig 4(e,f) proffering hexagonal pore morphologies, fig 4(b,d). Connectivity of the mesoporous architecture, via the assembly of ceria nanoparticles, is evident in both the atomistic model, fig 4(e), and the real material, fig 4(f).

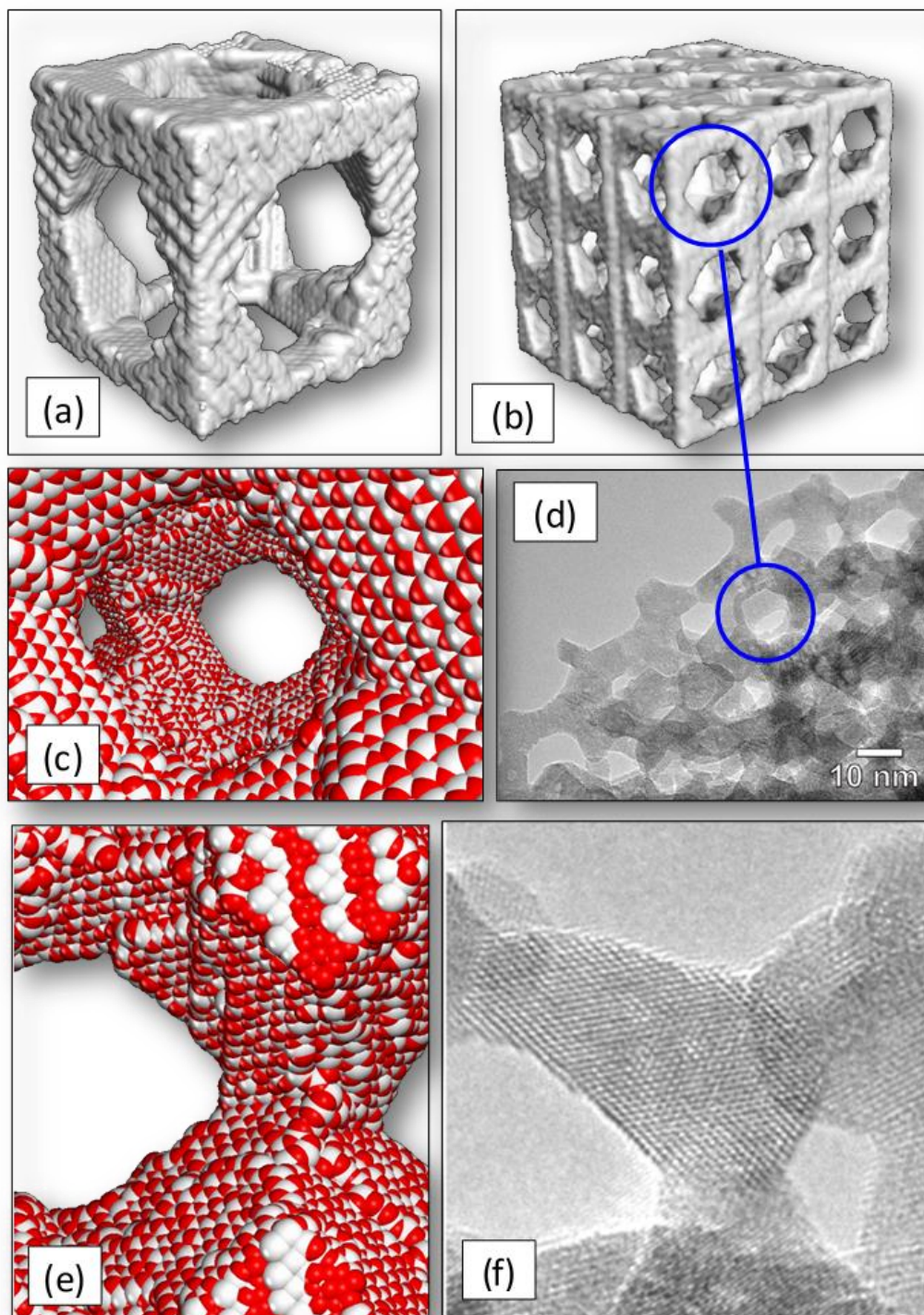


Figure 4 Atom-level models of mesoporous CeO₂ compared to the real material. (a) Unit cell of mesoporous ceria (model), (b) supercell comprising 9 unit cells to show the connectivity of pores. (c) model structure of an internal pore, (d) HRTEM of real mesoporous CeO₂, (e) atomistic model of a pillar comprising the pore wall, (f) HRTEM of the real material. (d) and (e) are taken with permission from ref [26]. Copyright American Chemical Society. Cerium is coloured white and oxygen is red. All images

depict atom positions (none are schematic); (a) and (b) are Connolly surface rendered models (solvent accessible surface area).

Defect Energies

Equipped with the atomistic models, oxygen vacancy formation energies were calculated to facilitate oxygen depletion levels of: 1, 2, 5, 10, 15 and 20%. Specifically, oxygen ions were removed, at random positions, from each nanostructure. For every O^{2-} ion removed, two Ce^{4+} ions, at random positions, were reduced to Ce^{3+} to facilitate charge neutrality. MD simulation, performed at 2000 K for 5 ns, was used to drive the oxygen vacancies to low energy positions within the lattice; each system was then cooled to 1K. High-temperature, 'long-duration' (5 ns) MD simulation was required because oxygen vacancies, created within the lattice at random positions, are unlikely located at the lowest energy positions. The MD simulation facilitates fast-ion conduction of the oxygen ions (and hence the vacancies), such that the vacancies are able to move to low energy positions. In particular, we found that surface oxygen vacancies migrated during the MD simulation to positions below the surface as predicted previously by Cormack and co-workers.²⁹ Similarly, the association energy between the oxygen vacancy and Ce^{3+} ions will drive the vacancy to be located near or adjacent to Ce^{3+} species.^{3,30,31}

Oxygen Depleted Nanostructures

The atomistic structures of the reduced nanoceria models are shown in fig 5 and figs. S7-S10. Analysis of the models, using molecular graphics, reveals that the fluorite structure is maintained for oxygen depletion levels spanning 1-20% for all nanostructures (polyhedral, cube, mesoporous). Moreover, the surface reconstruction, after oxygen depletion, was not so extensive as to destroy the surfaces exposed; the nanoparticle still exposes $CeO_2\{111\}$, $CeO_2\{110\}$ and $CeO_2\{100\}$ surfaces after 20% oxygen depletion, fig S8(a-f). Conversely, the oxygen sublattice is heavily perturbed when oxygen is depleted, fig 5(c). We attribute this to lattice relaxation around Ce^{3+} ions, which are larger than Ce^{4+} ions, and relaxation around the (oxygen) vacant sites. In the following section we describe the experiments used to determine whether the defect chemistry can be engineered into the real material.

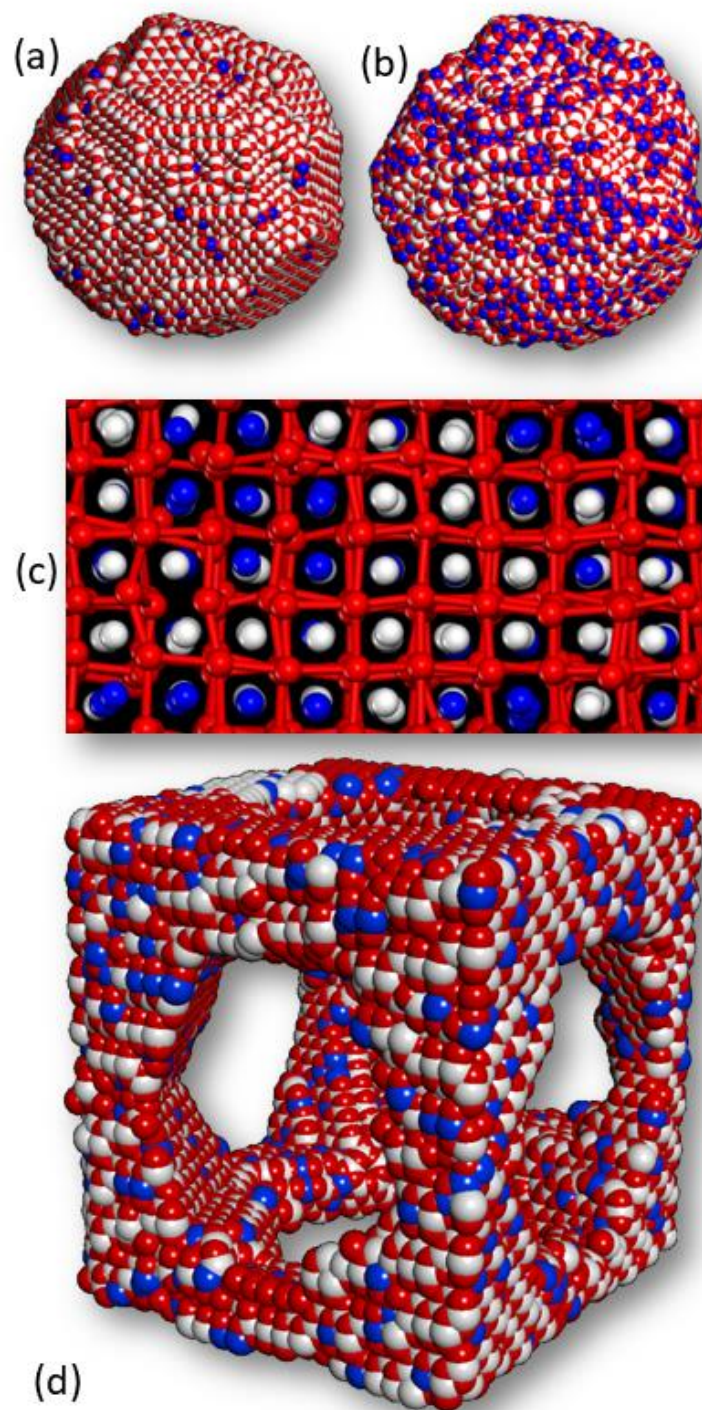


Figure 5 Models of reduced ceria nanostructures. (a) 13 nm polyhedral nanoparticle with 1% oxygen depletion. (b) 13 nm nanoparticle with 10% oxygen depletion. (c) Segment cut through (b) showing the oxygen sublattice disorder. (d) mesoporous ceria model with 5% oxygen depletion. Ce⁴⁺ is coloured white, Ce³⁺ is coloured blue and oxygen is red.

Experimental methods

Operando X-ray photoelectron spectroscopy (XPS) was performed on two different cerium oxide nanomaterials by introducing either H₂O (reduction) or O₂ (oxidation) into the reaction chamber to increase or decrease the vacancy concentration (and Ce⁴⁺/Ce³⁺ ratio) of the nanomaterials respectively. The nanoparticles were synthesized, with different surface Ce³⁺/Ce⁴⁺ ratios, using methods described previously and named CNP-1 (higher Ce³⁺, ref. ³²) and CNP-2 (lower Ce³⁺, ref. ¹⁶).

Photoemission spectra were recorded using a custom-built ambient pressure X-ray photoelectron spectrometer (AP-XPS) from SPECS Surface Nano Analysis GmbH, Germany. An analysis chamber with a base pressure of 5×10⁻¹⁰ mbar was equipped with an Al Kα X-ray tube (1486.7 eV) coupled to a Micro-FOCUS 600 monochromator (XR-MF). A volume-minimized reaction cell (15 cm³) inside the analysis chamber was attached to a differentially-pumped, electrostatic lens system and a PHOIBOS 150 hemispherical energy analyzer. The power of the X-ray source was set at 100 W, with an anode voltage and emission current of 15 kV and 6.7 mA, respectively. The X-ray beam was transmitted through a silicon nitride membrane window, which was incorporated into the reaction cell wall, and was incident at 54.7° to the sample surface normal. The X-ray beam had a 3 mm × 2 mm elliptical spot, as estimated from illumination of a phosphor screen. A detailed description of the experimental set-up of our operando XPS study was reported previously.³³ Binding energy calibration of the photoemission spectra were referred to the Au 4f_{7/5} peak at 84 eV and CasaXPS software used to assist peak fittings.

The ceria nanocrystal powder was pressed onto a pre-cleaned Au foil and loaded into ultra-high vacuum (UHV) conditions and kept for ~5 h prior to any further in-situ measurement. The same procedure was performed for each sample because ceria shows instability under UHV conditions and suffers self-reduction. Ultra-pure water was degassed by multiple freeze–pump–thaw cycles prior to use. Oxygen, with state purity of 99.993%, was sourced from Airgas. The purity of the reactants (water and oxygen) was monitored by a residual gas analyzer (RGA) mass spectrometer attached to one of the chambers of the differentially pumped system.

RESULTS

Here, we present the energies required to extract oxygen from the nanoceria catalysts as a function of oxygen depletion level. Intuitively, oxygen vacancy formation energies are linked with the activity of the catalyst.² We then use these energies to formulate the activity map. Finally, we show how the defect content of the nanoceria can be tuned experimentally to reach areas of optimum activity.

Defect Energies

The energies required to extract oxygen, for each of the ceria nanostructures, are shown in fig 6, following:



The figure reports the oxygen vacancy formation energies, per oxygen vacancy. Defect equilibria, pertaining to the reduction, are given in supporting material. The defect energies are similar to those calculated by Migani et al. who calculated the energy associated with extracting oxygen from ceria nanoparticles, up to 240 atoms (80 cerium, 120 oxygen) in size, using density functional theory.³⁴

Inspection of the figure reveals that activity towards oxidation *increases* in the order: Mesoporous - Nanocube - Large Nanoparticle - Small nanoparticle. For example, extracting oxygen from the small nanoparticle requires the least amount of energy and is therefore the most active nanoform towards oxidation. The figure also reveals that as oxygen is depleted, it becomes increasingly more difficult energetically to extract further oxygen (activity reduces) until a maximum is reached at about 10%. The smallest nanoparticle (3.5 nm) does not mirror the trend associated with the other nanostructures; there does not appear to be a maximum at oxygen depletion levels of 10% and our calculations reveal that it is easier to extract oxygen at 2% depletion compared to 1% depletion.

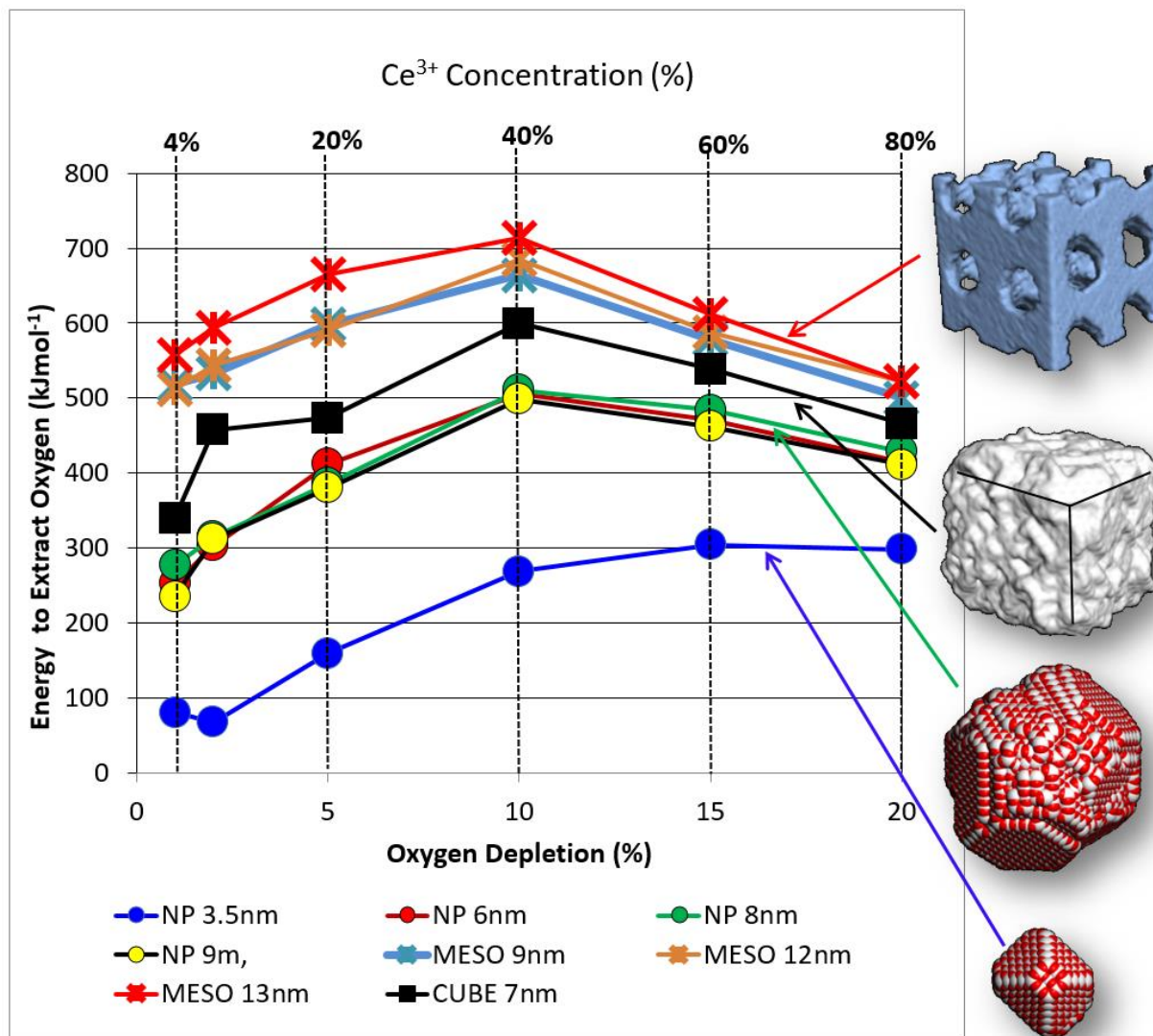
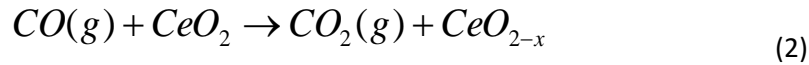


Figure 6 Oxygen Vacancy formation energies, calculated as a function of oxygen depletion for each of the nanostructures.

Oxidation

Equipped with the oxygen vacancy formation energies, one can calculate the thermodynamics associated with using the ceria catalyst to participate in 'any' oxidation or reduction reaction. We have chosen the oxidation of CO to CO₂ as an example. In particular, the CO extracts oxygen from the ceria catalyst to form CO₂ leaving an oxygen vacancy on the catalyst.¹ The reaction is shown in equation (2)

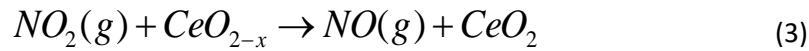


The energy associated with this reaction is simply the oxygen vacancy formation energy, equ. (1) plus the enthalpy associated with the oxidation of carbon monoxide to carbon dioxide, which was taken from standard thermodynamic tables:



Reduction

To act as a catalyst, the reduced ceria must source oxygen from another species to restore the depleted oxygen. Here, we have chosen the reduction of NO₂ to NO as an example:



Similarly, the energy associated with this reaction is calculated using the enthalpy associated with the reduction of NO₂ to NO, which was taken from standard thermodynamic tables:



Here, one takes the negative of the oxygen vacancy formation energy, because the oxygen content of the catalyst is being replenished. We note that 'any' other catalytic cycle can be considered by using values taken from standard thermodynamic tables.

Activity Map

The thermodynamic cycle, derived using equations (2) and (3), is shown in fig 7 and captures the thermodynamics of CO oxidation and NO₂ reduction together with the calculated oxygen vacancy formation energies, fig 6. Moreover, because oxygen vacancy formation energies, which are implicit within fig 7, are linked with the activity of the catalyst, the figure manifests as an activity map and reveals activity as a function of shape (particle, cube), defect content (oxygen depletion), architecture (mesoporous) and size (particle diameter, wall thickness). For example, inspection of the blue/red contours, fig 7(b), reveals that optimum activity of ceria towards reduction of NO₂ corresponds to mesoporous ceria with oxygen depletion levels around 10%; the contours further show that reducing the wall thickness reduces the activity.

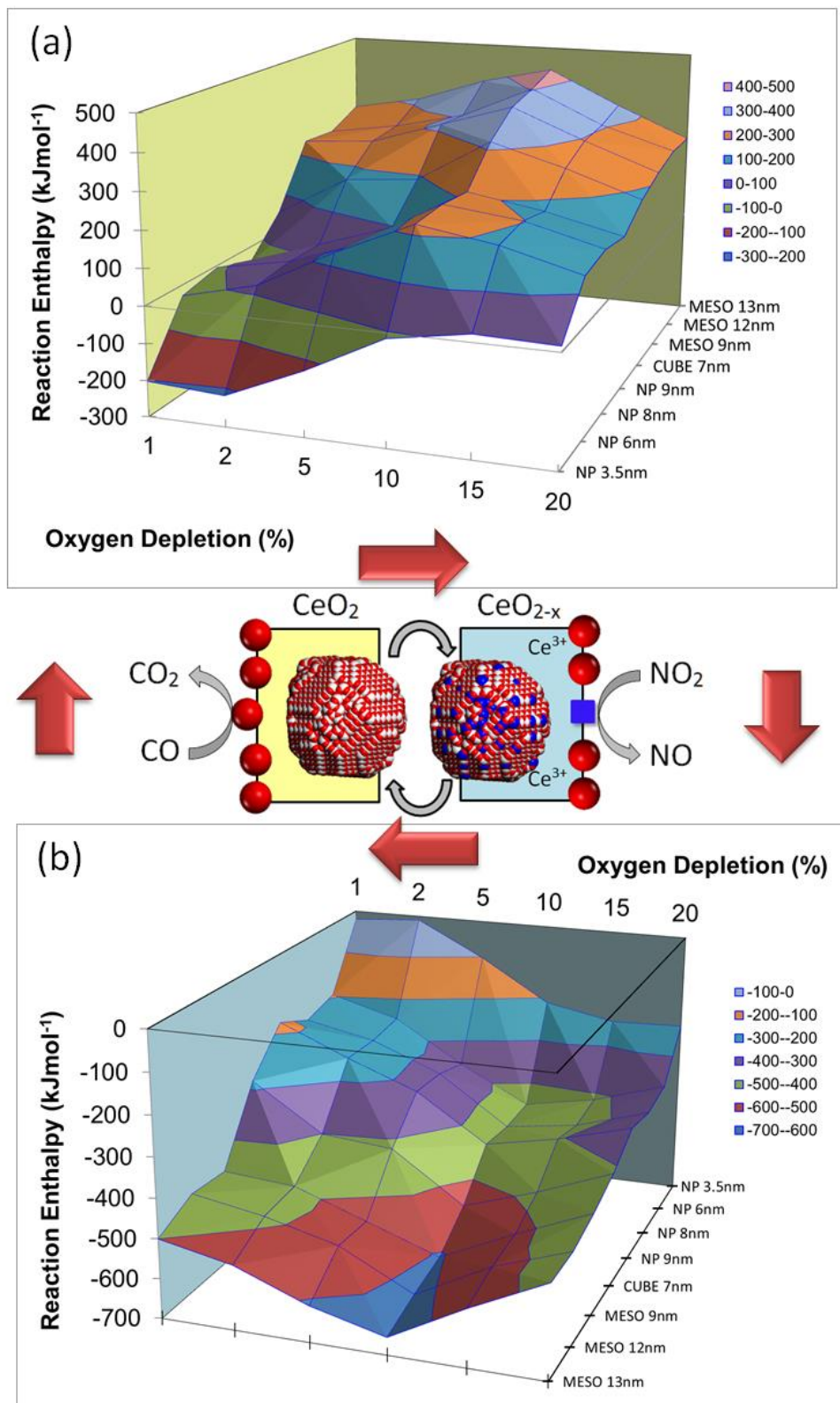


Figure 7 Activity map for nanoceria as a function of defect content, nanoarchitecture and size. Activity toward (a) CO oxidation (b) NO_2 reduction. The schematic at the centre illustrates the catalytic cycle.

Defect Engineering

Our simulations predict that the activity of nanoceria changes as a function of its defect concentration. However, activity tuning is only possible if the defect content can be engineered experimentally. Moreover, during an oxidation reaction, the oxygen content of the nanoceria will gradually be depleted, which might lead to a non-optimum defect state of the nanomaterial. Accordingly, it must be possible to control the defect content *during* a catalytic reaction.

The concentration of oxygen vacancies, measured under oxidizing (O_2) or reducing (H_2O) conditions, are presented in fig 8. The figure reveals that under oxygen, the Ce^{3+} concentration (and hence oxygen vacancy concentration) decreases. Similarly, when nanoceria is exposed to H_2O , the Ce^{3+} concentration increases. Our experiments reveal that the defect chemistry of nanoceria can indeed be engineered to control the activity of the nanomaterial as predicted. The defect concentrations, fig 8, were derived from photoemission spectra, figs S11, S12; further details can be found in supporting material.

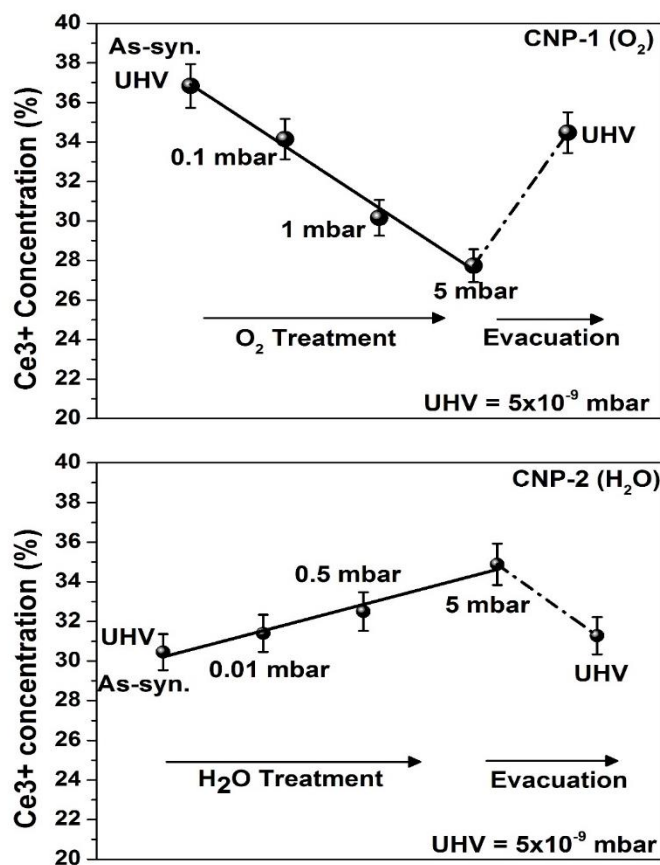


Figure 8 Percentage of Ce^{3+} calculated from integrated area of $Ce3d$ spectrum, fig S11, S12, as a function of O_2 (top) and H_2O (bottom) gas pressure for CNP-1 and CNP-2.

DISCUSSION

The oxygen storage capacity (OSC) of ceria is the amount of oxygen that ceria can liberate during, for example, an oxidative reaction, $\text{CeO}_2 - \text{O}_2 \rightarrow \text{CeO}_{2-x}$.¹⁸ Our simulations reveal, fig 6, that as oxygen is gradually depleted, it becomes energetically more difficult to extract further oxygen. We propose that the OSC of ceria corresponds to the level of depletion where it is energetically prohibitive to extract further oxygen from the material. Fig 6 also reveals that the oxidative activity of the catalyst decreases during an oxidation reaction because it becomes gradually more difficult to extract oxygen. Our simulations therefore reveal a 'window of catalytic operation', where the activity of the catalyst can be controlled by operating at different points within this window. We show experimentally, fig 8, how one can operate in different parts of the window by manipulating the oxygen vacancy concentration and hence oxygen content of the catalyst by changing the oxygen and/or H₂O partial pressures. Experimentally, we find that the window of operation for ceria nanoparticles spans: 28-37% Ce³⁺, which corresponds to oxygen depletion levels of 7 - 9.25% using O₂ and H₂O. The somewhat narrow range emanates from the difficulty in preparing fully oxidized nanoceria, CeO₂.

Our simulations also suggest that the OSC can change depending upon the particular chemical reaction being performed. For example, the free energy of the reaction comprises the reaction enthalpy added to the vacancy formation energy (such as equation 2). As more oxygen is extracted so the vacancy formation energy increases; this would continue until a positive value for the free energy were reached. However, if an alternative reaction, with a more negative reaction enthalpy, were performed, we propose that the extra energy would offset the vacancy formation energy and hence more oxygen could potentially be extracted.

The maximum in the vacancy formation energy, for all nanostructures other than the 3.5 nm nanoparticle, fig 6, indicates that at about 10% oxygen depletion, extracting further oxygen would become energetically easier. Conversely, we note that the system is approaching the limit of oxygen depletion where all the Ce⁴⁺ is reduced to Ce³⁺ (25% oxygen depletion). Moreover, experimentally, we achieved oxygen depletion levels of up to 9.25%. In addition, we caution, that the real system is more complex. For example, oxygen extraction from nanoceria {100} surfaces is energetically easier than {111} surfaces and therefore kinetic processes will contribute to the OSC. Transport of oxygen (oxygen ion conductivity) is also central to OSC

to ensure that vacancies, created on the surface of the catalyst, are 'quickly' replaced by oxygen ions from within the structure. Entropic contributions, which were not considered in this present study, may also play a key role.

A catalyst cannot influence the thermodynamics of a reaction – only the kinetics. Conversely, figs. 6 and 7 suggests that the ceria catalyst changes the thermodynamics of the reaction. For example, fig 6 shows that the enthalpies required to oxidise CO to CO₂, using 3.5 nm ceria nanoparticles with oxygen depletion levels at 1%, is -203 kJmol⁻¹. As the oxidation of CO to CO₂ progresses, the nanoparticle becomes more oxygen deficient; at 10% oxygen depletion, the reaction enthalpy reduces to -15 kJmol⁻¹ indicating that the catalyst can influence significantly the thermodynamics of the reaction. Similarly, the energy required to reduce NO₂ to NO, using 3.5 nm nanoparticles of ceria and 10% oxygen depletion, is -211 kJmol⁻¹, which reduces to -23 kJmol⁻¹ as the oxygen is replenished and the ceria catalyst is once again 1% oxygen deficient. The thermodynamic cycle (assuming the ceria catalyst starts and ends at 1% oxygen depletion) starts with a reaction enthalpy of -203 kJmol⁻¹ and ends at a reaction enthalpy of -23 kJmol⁻¹. Accordingly, the total reaction energy is -226 kJmol⁻¹, which is equivalent to the enthalpy associated with the two reactions $\text{CO} + \text{O}_2 \rightarrow \text{CO}_2$ (-282.75 eV) + $\text{NO}_2 - \frac{1}{2}\text{O}_2 \rightarrow \text{NO}$ (+56.94 eV) = -226 kJmol⁻¹. The catalyst does not change the thermodynamics of the whole 'macroscopic' cycle; rather it is only the thermodynamic quantities associated with each 'microscopic' reaction that are different.

A nanomaterial-based catalytic system will comprise a considerable number of nano-objects, which will likely exist at different (distribution) levels of oxygen depletion, particle size and perhaps particle shape. The 'macroscopic' catalysis manifests as the summation of all the different 'microscopic' thermodynamic processes operating for each nano-object at their particular level of oxygen depletion. For a complete cycle, which renders the catalyst unchanged, the catalyst makes no contribution to the thermodynamic quantities. Conversely, the kinetics of the reaction will be driven by the thermodynamics associated with each 'microscopic' process. In particular, the activation energy barrier is (intuitively) linked to the energy required to extract oxygen from the catalyst; Aryanpour, Khetan and Pitsch have shown that the oxygen vacancy formation energy is a 'simple yet powerful activity predictor for catalytic reactions on ceria'.² We therefore propose that the map, fig 7, can be used to predict the activity of the particular ceria catalyst as a function of oxygen depletion. Examination of the activity map reveals, for example:

- The activity of nanoceria is influenced profoundly by its oxygen content. In particular, as oxygen is gradually depleted, so the energy required to extract further oxygen increases, rendering the nanoceria less active towards oxidative catalysis. Specifically, the activity changes *during* the catalytic reaction.
- The oxygen storage capacity (OSC) of nanoceria is central to oxidative catalysis. Increasing the OSC of ceria is therefore important.³⁵ We predict that it becomes increasingly more difficult to continue to extract oxygen, which helps explain the challenges associated with maximizing OSC.
- The activity is influenced by the size of the nanomaterial (diameter or wall thickness). In particular, our calculations show that it is easier (energetically) to extract oxygen from the 3.5nm particle compared to the larger nanoparticles. This is consistent with the findings of Migani and co-workers, who hypothesised that 'a minimum in the oxygen vacancy formation energy as a function of nanoparticle size'.³⁶ Moreover, Deshpande and co-workers find a link between particle size and level of oxygen depletion within ceria nanoparticles.¹⁷
- For 3.5 nm ceria nanoparticles and oxygen depletion levels of >5% (80% Ce⁴⁺/20% Ce³⁺), it becomes energetically more favourable to replenish the oxygen depleted (from NO₂) rather than oxidising more CO to CO₂.
- 3.5 nm ceria nanoparticles are most active towards CO oxidation at oxygen depletion levels of 2% (92%Ce⁴⁺/8%Ce³⁺).

Such activity mapping can be applied to any oxidation/reduction process that utilise nanoceria catalysts. In particular, the calculated activity map, used to describe our operando XPS study for O₂ (oxidation) and H₂O (reduction), is presented in fig S13. Our strategy is general in that the study provides a framework to calculate activity maps of other technologically important materials.

Creating an activity map is analogous to the way one uses tabulated thermodynamic data to determine, for example, the enthalpy or free energy associated with a particular chemical reaction. For example, the thermodynamic quantities, pertaining to the particular reaction of interest (taken from thermodynamic data tables), simply need to be introduced (such as equ. (2) – oxidation and equ. (3) – reduction); a spreadsheet can then be used to facilitate the automated generation of the activity map, as was

performed to generate fig 7. An interactive activity map is available as supporting information. Here, enthalpy values for ‘any’ oxidation/reduction can be introduced and the activity map is redrawn. Our experiments reveal that it is possible to engineer defect concentration into nanoceria, as expected, to enable domains of optimised activity, such as those predicted in fig 7, to be reached.

CONCLUSIONS

Molecular Dynamics simulation was used to generate atomistic models of ceria nanoparticles (3.5 – 9 nm), ceria nanocube (7 nm) and mesoporous ceria (wall thickness 3-10 nm) with simple cubic and face-centered cubic architectures. The model structures comprise a variety of microstructural features including grain-boundaries and dislocations and show quantitative structural accord with nanoceria fabricated experimentally.

The models were used to calculate the energy associated with using nanoceria to catalyse the oxidation of CO to CO₂ and the reduction of NO₂ to NO. Specifically, oxygen vacancy formation energies were calculated, which have been shown to be a ‘simple yet powerful activity predictor for catalytic reactions on ceria’. As oxygen is extracted from the nanoceria to oxidise CO to CO₂, the oxygen content of the catalyst is gradually depleted; the oxygen content is subsequently replenished during the reduction reaction, NO₂ – ½O₂ → NO. Accordingly, an activity map was generated as a function of the defect concentration of the ceria catalyst spanning: CeO_{2-x}, where x=0 to 0.4.

The calculated activity map was used to proffer predictions for experiment. Specifically, we reveal that the activity of nanoceria is influenced profoundly by its defect content. Similarly, size (particle diameter, mesoporous wall thickness) and nanostructuring (particle, cube, mesoporous, morphology and surfaces exposed) are key drivers of catalytic activity. Experimentally, we show that the defect chemistry of nanoceria can be finely and reversibly tuned, during a chemical reaction, by exposing the nanomaterial to either oxidising or reducing environments.

ACKNOWLEDGEMENTS

Barry Blight for useful discussion; EPSRC: EP/H001220; U.S. Department of Energy Office of Science, Office of Basic Energy Sciences under Award Number DE-FC02-04ER15533 (NDRL no: 5104).

ASSOCIATED CONTENT

Supporting Information Atomistic models of nanostructures, methods for generating atomistic models, microstructural features, defect equilibria, photoemission spectra, interactive activity map.

AUTHOR INFORMATION

Corresponding Author

* Dean C. Sayle d.c.sayle@kent.ac.uk

REFERENCES

¹ Reed, K.; Cormack, A.; Kulkarni, A.; Mayton, M.; Sayle, D.; Klaessig, F. and Stadler, B.
Exploring the Properties and Applications of Nanoceria: Is There Still Plenty of Room at the Bottom?
Environ. Sci.: Nano, 1, 390, 2014

² Aryanpour, M.; Khetan, A. and Pitsch, H.
Activity Descriptor for Catalytic Reactions on Doped Cerium Oxide
ACS Catal., 2013, 3, 1253

³ Sayle, T. X. T.; Parker, S. C. and Catlow, C. R. A.
The Role of Oxygen Vacancies on Ceria Surfaces in the Oxidation of Carbon-monoxide
Surf. Sci., 1994, 316, 329

⁴ Conesa, J. C.
Computer modelling of surfaces and defects on cerium dioxide
Surf Sci., 1995, 339, 337

⁵ Mullins, D.
The surface chemistry of cerium oxide
Surf Sci. Reports, 2015, 70, 42

⁶ Wang, X.; Jiang, Z.; Zheng, B.; Xie, Z. and Zheng, L.
Synthesis and shape-dependent catalytic properties of CeO₂ nanocubes and truncated octahedra
Cryst. Eng. Comm., 2012, 14, 7579

⁷ Na, T.; Jingyue, L. and Wenjie, S.
Tuning the shape of ceria nanomaterials for catalytic applications
Chinese J. Catalysis, 2013, 34, 838

⁸ Sreeremya, T.; Krishnan, A.; Remani, K.; Patil, K.; Brougham, D. and Ghosh, S.
Shape-Selective Oriented Cerium Oxide Nanocrystals Permit Assessment of the Effect of the Exposed Facets on Catalytic Activity and Oxygen Storage Capacity
ACS Appl. Mater. Interfaces, 2015, 7, 8545

-
- ⁹ Liu, X.; Zhou, K.; Wang, L.; Wang, B. and Li, Y.
Oxygen Vacancy Clusters Promoting Reducibility and Activity of Ceria Nanorods
J. Am. Chem. Soc. 2009, **131**, 3140
- ¹⁰ Lin, Y.; Wu, Z.; Wen, J.; Poepelmeier, K. and Marks, L.
Imaging the Atomic Surface Structures of CeO₂ Nanoparticles
Nanotechnology Lett. 2014, **14**, 191
- ¹¹ Florea, I.; Feral-Martin, C.; Majimel, J.; Ihiawakrim, D.; Hirlimann, C. and Ersen, O.
Three-Dimensional Tomographic Analyses of CeO₂ Nanoparticles
Cryst. Growth Des. 2013, **13**, 1110
- ¹² Kaneko, K.; Inoke, K.; Freitag, B.; Hungria, A.; Midgley, P.; Hansen, T.; Zhang, J.; Ohara, S. and Adschiri, T.
Structural and Morphological Characterization of Cerium Oxide Nanocrystals Prepared by Hydrothermal Synthesis
Nano Lett., 2007, **7**, 421
- ¹³ Zhang, J.; Kumagai, H.; Yamamura, K.; Ohara, S.; Takami, S.; Morikawa, A.; Shinjoh, H.; Kaneko, K.; Adschiri, T. and Suda, A.
Extra-Low-Temperature Oxygen Storage Capacity of CeO₂ Nanocrystals with Cubic Facets
Nano Lett. 2011, **11**, 361
- ¹⁴ Sayle, T.; Parker, S. and Sayle, D.
Oxidising CO to CO₂ using Ceria nanoparticles
Phys. Chem. Chem. Phys., 2005, **7**, 2936
- ¹⁵ Sayle, T.; Cantoni, M.; Umanada, M.; Parker, S.; Hall, S.; Moebus, G.; Molinari, M.; Reid, D.; Seal, S. and Sayle, D.
Strain and Architecture-Tuned Reactivity in Ceria Nanostructures; Enhanced Catalytic Oxidation of CO to CO₂
Chem. Mater., 2012, **24**, 1811
- ¹⁶ Das, S.; Singh, S.; Dowding, J. M.; Oommenc, S.; Kumar, A.; Sayle, T. X.T.; Saraf, S.; Patra, C. R.; Vlahakis, N. E.; Sayle, D. C.; Self, W. T. and Seal, S.
The induction of angiogenesis by cerium oxide nanoparticles through the modulation of oxygen in intracellular environments
Biomaterials, 2012, **33**, 7746
- ¹⁷ Deshpande, S.; Patil, S.; Kuchibhatla, S. V. N. T. and Seal, S.
Size dependency variation in lattice parameter and valency states in nanocrystalline cerium oxide
Appl. Phys. Lett. 2005, **87**, 133113
- ¹⁸ Montini, T.; Melchionna, M.; Monai, M. and Fornasiero, P.
Fundamentals and Catalytic Applications of CeO₂-Based Materials
Chem. Rev., **2016**, **116** (10), pp 5987–6041
- ¹⁹ Lawrence, N. J.; Brewer, J. R.; Wang, L.; Wu, T. S.; Wells-Kingsbury, J.; Ihrig, M. M.; Wang, G. H.; Soo, Y. L.; Mei, W. N. and Cheung, C. L.
Defect Engineering in Cubic Cerium Oxide Nanostructures for Catalytic Oxidation
NanoLett., 2011, **11**, 2666
- ²⁰ Li, Y. and Shen, W.
Morphology-dependent nanocatalysts: Rod-shaped oxides
Chem. Soc. Rev., 2014, **43**, 1543
- ²¹ Namai, Y.; Fukui, K. and Iwasawa, Y.
The dynamic behaviour of CH₃OH and NO₂ adsorbed on CeO₂(111) studied by noncontact atomic force microscopy
Nanotechnology, 2004, **15**, S49
- ²² Vile, G.; Colussi, S. Krumeich, F.; Trovarelli, A. and Perez-Ramirez, J.

Opposite Face Sensitivity of CeO₂ in Hydrogenation and Oxidation Catalysis
Angew. Chem. Int. Ed. 2014, 53, 12069

²³ Roy, N.; Sohn, Y. and Pradhan, D.
Synergy of Low-Energy {101} and High-Energy {001} TiO₂ Crystal Facets for Enhanced Photocatalysis
ACS NANO, 2013, 7, 2532

²⁴ Smith, W. Forester, T. R. and Todorov, I. T.
http://www.ccp5.ac.uk/DL_POLY_CLASSIC/

²⁵ Ji, P.; Zhang, J.; Chen, F. and Anpo, M.
Ordered Mesoporous CeO₂ Synthesized by Nanocasting from Cubic Ia3d Mesoporous MCM-48 Silica: Formation, Characterization and Photocatalytic Activity
J. Phys. Chem. C, 2008, 112, 17809-17813

²⁶ Hartmann, P.; Brezesinski, T.; Sann, J.; Lotnyk, A.; Eufinger, J.; Kienle, L. and Janek, J.
Defect Chemistry of Oxide Nanomaterials with High Surface Area: Ordered Mesoporous Thin Films of the Oxygen Storage Catalyst CeO₂-ZrO₂
ACS Nano, 2013, 7, 2999

²⁷ Goris, B.; Turner, S.; Bals, S. and Van Tendeloo, G.
Three-Dimensional Valency Mapping in Ceria Nanocrystals
ACS Nano, 2014, 8, 10878

²⁸ Tan, J.; Tan, H.; Boothroyd, C.; Foo, Y.; He, C. and Lin, M.
Three-Dimensional Structure of CeO₂ Nanocrystals
J. Phys. Chem. C 2011, 115, 3544

²⁹ A. N. Cormack, S. Lamphier, Bu Wang, T. Gubb, K. Reed
Simulations of ceria nanoparticles
Proc. R. Soc. A 2015, 471, 20150218; DOI: 10.1098

³⁰ Torbrügge, S. and Reichling, M.
Evidence of Subsurface Oxygen Vacancy Ordering on Reduced CeO₂(111)
Phys. Rev. Lett., 2007, 99, 056101

³¹ Murgida, G. E. And Ganduglia-Pirovano, M. V.
Evidence for Subsurface Ordering of Oxygen Vacancies on the Reduced CeO₂(111) Surface Using Density-Functional and Statistical Calculations
Phys. Rev. Lett., 2013 110, 246101

³² Tamilselvan, S.; Das, S.; Kumar, A.; Reid, D. L.; Gupta, A.; Sayle, D. C. and Seal, S.
Morphological phase diagram of biocatalytically active ceria nanostructures as a function of processing variables and their properties.
ChemPlusChem 2013, 78, 1446

³³ Zhang, X., and S. Ptasinska.
"Dissociative Adsorption of Water on an H₂O/GaAs(100) Interface: In Situ Near-Ambient Pressure XPS Studies."
Journal of Physical Chemistry C 2014, 118, 4259

³⁴ Migani, A.; Vayssilov, G. N.; Bromley, S. T.; Illas, F. and Neyman, K. M.
Greatly facilitated oxygen vacancy formation in ceria nanocrystallites
Chem. Commun., 2010, 46, 5936-5938

³⁵ Ishikawa, Y.; Takeda, M. Tsukimoto, S.; Nakayama, K. S. and Asao, N.

Cerium Oxide Nanorods with Unprecedented Low-Temperature Oxygen Storage Capacity
Adv. Mater. 2015, 28, 1467-1471

³⁶ Migani, A.; Vayssilov, G. N.; Bromley, S. T.; Illas, F. and Neyman, K. M.

Dramatic reduction of the oxygen vacancy formation energy in ceria particles: a possible key to their remarkable reactivity at the nanoscale

J. Mater. Chem., 2010, 20, 10535